© 2021. Published by The Company of Biologists Ltd | Journal of Experimental Biology (2021) 224, jeb238808. doi:10.1242/jeb.238808

RESEARCH ARTICLE

Beyond the Kármán gait: knifefish swimming in periodic and irregular vortex streets

Victor M. Ortega-Jiménez* and Christopher P. Sanford

ABSTRACT

Neotropical freshwater fishes such as knifefishes are commonly faced with navigating intense and highly unsteady streams. However, our knowledge on locomotion in apteronotids comes from laminar flows, where the ribbon fin dominates over the pectoral fins or body bending. Here, we studied the 3D kinematics and swimming control of seven black ghost knifefish (*Apteronotus albifrons*) moving in laminar flows (flow speed $U_\infty \approx 1$–5 BL s^{-1}) and in periodic vortex streets ($U_\infty \approx 2$–4 BL s^{-1}). Two different cylinders (~2 and ~3 cm diameter) were used to generate the latter. Additionally, fish were exposed to an irregular wake produced by a free oscillating cylinder (~2 cm diameter; $U_\infty \approx 2$ BL s^{-1}). In laminar flows, knifefish mainly used their ribbon fin, with wave frequency, speed and acceleration increasing with U_∞. In contrast, knifefish swimming behind a fixed cylinder increased the use of pectoral fins, which resulted in changes in body orientation that mimicked steady backward swimming. Meanwhile, individuals behind the oscillating cylinder presented a combination of body bending and ribbon and pectoral fin movements that counteract the out-of-phase yaw oscillations induced by the irregular shedding of vortices. We corroborated passive out-of-phase oscillations by placing a printed knifefish model just downstream of the moving cylinder, but when placed one cylinder diameter downstream, the model oscillated in phase. Thus, the wake left behind an oscillating body is more challenging than a periodic vortex shedding for an animal located downstream, which may have consequences on inter- and intra-specific interactions.

KEY WORDS: Unsteady locomotion, Swimming control, Vortex-induced vibration, Kármán vortex streets, Black ghost knifefish

INTRODUCTION

Apteronotid knifefishes are neotropical freshwater organisms thriving in the fast-flowing and turbulent waters of Central and South American streams, including the Amazon River. This group of fishes has received significant attention for their capacity of tissue regeneration (Sîrbulescu et al., 2009), and electro-communication signaling (Thompson et al., 2018), but mostly because they possess outstanding swimming abilities. Knifefishes can move in any direction regarding their body orientation, or stay still in mid-water by flapping and oscillating their multi-rayed and elongated anal fin, while keeping a straight body posture (Blake, 1983; Ruiz-Torres et al., 2013; Sefati et al., 2013; Youngerman et al., 2014). However, our knowledge of knifefish biomechanics and hydrodynamics has been limited to laminar flows, which differs from the challenging and unsteady conditions they commonly encounter in the wild. *Apteronotus bonapartii*, for example, is mostly found in intense flowing waters (see Crampton, 1998). Furthermore, apteronotids live in complex environments (e.g. roots, logs and rocks) and often have nocturnal exploratory incursions at the shore from their diurnal refuges located in deeper waters (Steinbach, 1970). Thus, it is likely that knifefishes partition the use of pectoral fins, the ribbon fin and body bending to maximize efficiency when dealing with such unsteady flow environments.

The effects produced by unsteady flows on animals has been explored on both flying (Tucker, 1972; Combes and Dudley, 2009; Ortega-Jimenez et al., 2013, 2014, 2016) and swimming organisms (Liao et al., 2003a,b; Liao, 2007; Yuan and Hu, 2017). Most studies have focused on the effects produced by the classical von Kármán vortex street, a regular pattern of counter-rotating eddies downstream produced by a rigid body (e.g. a cylinder). Animal fliers, such as birds and insects that are dealing with gravity produce large lift forces and high flapping frequencies to remain airborne, which results in higher energetic cost and degraded flight performance in larger vortex wakes. Effects on animal fliers become even more exaggerated at higher flow speeds or when closer to the perturbation (see Ortega-Jimenez et al., 2016). In contrast, swimmers such as trout or tadpoles rely primarily on body undulations (i.e. the Kármán gait) to produce thrust in overcoming drag, and reduce energetic costs by swimming in vortex shedding (Liao et al., 2003b). However, this gait is highly dependent on flow speed, body length and body undulation frequency (Akanyeti and Liao, 2013; Yuan and Hu, 2017; but see Maia et al., 2015). It is notable that animal fliers, in spite of differences in morphology, mainly use their wings to navigate through the air, while fishes rely on the hydrodynamic forces generated by any combination of body undulations, median and/or paired fin oscillations or undulations (Lauder, 2015). To date, what we know about swimming performance of fishes in unsteady flow conditions comes from investigations of taxa that rely primarily on undulating the body. Thus, it remains largely unknown how groups such as apteronotids that use alternate means of propulsion deal with turbulent flow environments.

In natural systems, flow perturbations tend to be more complex and turbulent than the wakes left by fixed bluff bodies. This is because physical structures such as aquatic plants, roots, submerged logs and loose rocks tend to oscillate owing to a phenomenon called vortex-induced vibration (see Williamson and Govardhan, 2004). These vibrations result in an irregular pattern of vortex shedding that can have pronounced impacts on fish locomotion, which may differ substantially from those produced by Kármán vortex streets. However, the effects of irregular wakes generated by free oscillating bodies has not yet been explored in swimming animals.

Here, we analyzed the 3D kinematics and locomotory control of the black ghost knifefish (*Apteronotus albifrons*) swimming in three different flow conditions at varied speeds: in steady flows, in

Department of Ecology, Evolution, and Organismal Biology, Kennesaw State University, Kennesaw, GA 30144, USA.

*Author for correspondence (ornithopterus@gmail.com)

V.M.O., 0000-0003-0024-5086

Received 5 October 2020; Accepted 25 March 2021

Journal of Experimental Biology (2021) 224, jeb238808. doi:10.1242/jeb.238808

List of symbols and abbreviations

a_{RF}	ribbon fin wave acceleration
F_{drag}	drag force
I_t	turbulence intensity
L_{RF}	stroke amplitude of the ribbon fin
n_{PF}	pectoral fin stroke frequency
n_{RF}	ribbon fin wave frequency
PIV	particle image velocimetry
P_{thrust}	power
Re_b	Reynolds number based on the body
Re_{cyl}	Reynolds number based on the cylinder
St_{RF}	Strouhal number based on the ribbon fin
U_∞	flow speed
U_f	average flow speed
U_w	cylinder wake velocity
V_{RF}	ribbon fin wave speed
$V_{RF,max}$	maximum ribbon fin wave speed
β_b	pitch
γ_b	yaw
δ_{PF}	pectoral fin asymmetry
λ_{RF}	ribbon fin wave length
Φ_{PF}	pectoral fin stroke amplitude
Φ_{RF}	ribbon fin wave amplitude
χ_b	body bending
Ψ_b	roll

periodic vortex streets (two different vortex sizes), and in an irregular vortex shedding generated by a free, oscillating cylinder. The main goal of this study was to characterize the locomotion strategies and fluid dynamics associated with knifefish swimming in environments that more realistically reflect natural conditions. Using a knifefish printed model, we also provide a clearer picture of the role of different control appendages used in aquatic locomotion in response to complex and unsteady flows. This study also provides insights into potential ecological consequences of animals moving and interacting in complex and unsteady flows.

MATERIALS AND METHODS

Fish training

Seven black ghost knifefish [*Apteronotus albifrons* (Linnaeus 1766)] were obtained from a commercial pet supplier in Kennesaw, GA, USA. Individuals had a body length, pectoral fin length, pectoral fin area and pectoral fin chord of 9±1 cm, 1.0±0.1 cm, 0.4±0.1 cm^2 and 4.6±0.4 mm, respectively (means±s.d.). Also, the ribbon fin length, height and perimeter were 5.6±0.4 cm, 5±1 mm and 14±1 cm, respectively. Each individual was kept in a 151.4 liter tank with a pH of 7–8 and a water temperature of 25–26°C. Fish were fed frozen blood worms *ad libitum*. Before experiments, individuals were trained for a week to feed from a small feeder. The feeder was made of a clear plastic tube of 2.5 mm diameter and 1 cm length. A small hole (1 mm) in the middle of the feeder was made to encourage the fish to station hold (Fig. 1). Training was performed in a swim tunnel (Loligo® Systems, swim-90; test section 70×20×20 cm). It is important to note that this feeding method is commonly used in animal flying research (see Ortega-Jimenez et al., 2016) and permits consistent systematic comparisons among experimental treatments. Furthermore, this method is appropriate for knifefish because they commonly search for food using extensive exploration (V.M.O.-J., personal observation). During trials, the feeder was placed in the middle of the flume test section and ∼7 cm from the bottom.

After training, individuals were exposed to different varied experimental flow conditions in a random order (Fig. 1). These trials consisted of feeding and swimming sessions of ∼5 min, for each of the seven subjects, over 4 weeks. Fish were starved for the 2 days prior to the onset of swim trials. Each individual was exposed to the nine laminar conditions (see below sample size for higher speeds), two large cylinder conditions, four small cylinder conditions and one oscillating cylinder condition in a random order, with 20 min gaps between each trial. For laminar conditions, we tested nine different flow speeds: −1.4, 1.4, 1.8, 2.5, 3.0, 3.6, 3.9, 4.3 and 4.6 body lengths s^{-1} (BL s^{-1}). Negative and positive values denote backward and forward swimming, respectively. Notice that at higher forward speeds, only six individuals could swim and feed at 4.3 BL s^{-1}, while two were able to do so at 4.6 BL s^{-1}. To generate a von Kármán street, we use two different fixed cylinders: one large (2.6 cm diameter and 37 cm length) and one small (1.6 cm diameter and 37 cm length). Flow speeds tested for the large cylinder were 1.8 and 2.5 BL s^{-1}, and for the small cylinder were 1.8, 2.5, 3 and 3.6 BL s^{-1}. The wake produced by a free oscillating cylinder (1.6 cm diameter) was only tested at 1.8 BL s^{-1}.

Ethics statement

All methods were carried out in accordance with relevant federal guidelines and regulations. All training and experimental procedures were approved by Kennesaw State University's Institutional Animal Care and Use Committee (ACUP 20-008), and no animals were killed for this study.

Three-dimensional filming and digitization

We used two synchronized cameras (Fastec HiSpec 4) filming at 200 frames s^{-1} covering ventral and side views of the fish in the swim tunnel, respectively. Cameras were 3D calibrated using a direct linear transformation (DLT) method applied to a 24-point cube frame. We only used trials where fish were constantly feeding in the artificial feeder for at least ∼5 s. We analyzed up to 16 trials (see sample size for each trial in Table 1), each of length ∼2 s, and then digitized at the frame rate of 200 Hz. A total of ten 3D coordinates were collected for each frame for subsequent analysis (Fig. 1; Fig. S3).

Using the calibrated video sequences, we digitized the tip of the head, the tail and both pectoral fins, as well as the base of each pectoral fin and a mid-point in the midline of the ribbon fin base located between the head and the tail (yellow dots in Fig. 1). For the ribbon fin, we digitized the tip and base at the midline, and the tip of the trough formed by the ribbon fin wave (see green dot in Fig. 1A). The digitized points were used to calculate averages of pitch, yaw, roll, pectoral fin frequency, pectoral fin amplitude, pectoral fin asymmetry, ribbon fin frequency and ribbon fin amplitude (for details, see Fig. S3). We calculated the wave speed and acceleration of the ribbon fin from the first and second derivatives of a mean squared error quintic spline function (Walker, 1998) applied to the temporal series of the digitized wave trough. Ribbon fin wave length was calculated using the ribbon fin wave speed divided by ribbon fin frequency. The kinematics of only the left pectoral fin was calculated because it was visible in both cameras. Similarly, average pectoral fin asymmetry was calculated from the ventral view. For the latter, we use the angle that resulted between the vector formed by both pectoral fins and a vector perpendicular to the body (Fig. S3). Calibration and digitization were performed using MATLAB code (available at http://biomech.web.unc.edu/dltdv/).

Digital particle image velocimetry (DPIV) on flow and ribbon fin wake

A class-4 laser (Opto Engine LLC, 532 nm, 5 W) was used to produce a horizontal light sheet to illuminate plastic beads (50 µm)

Journal of Experimental Biology (2021) 224, jeb238808. doi:10.1242/jeb.238808

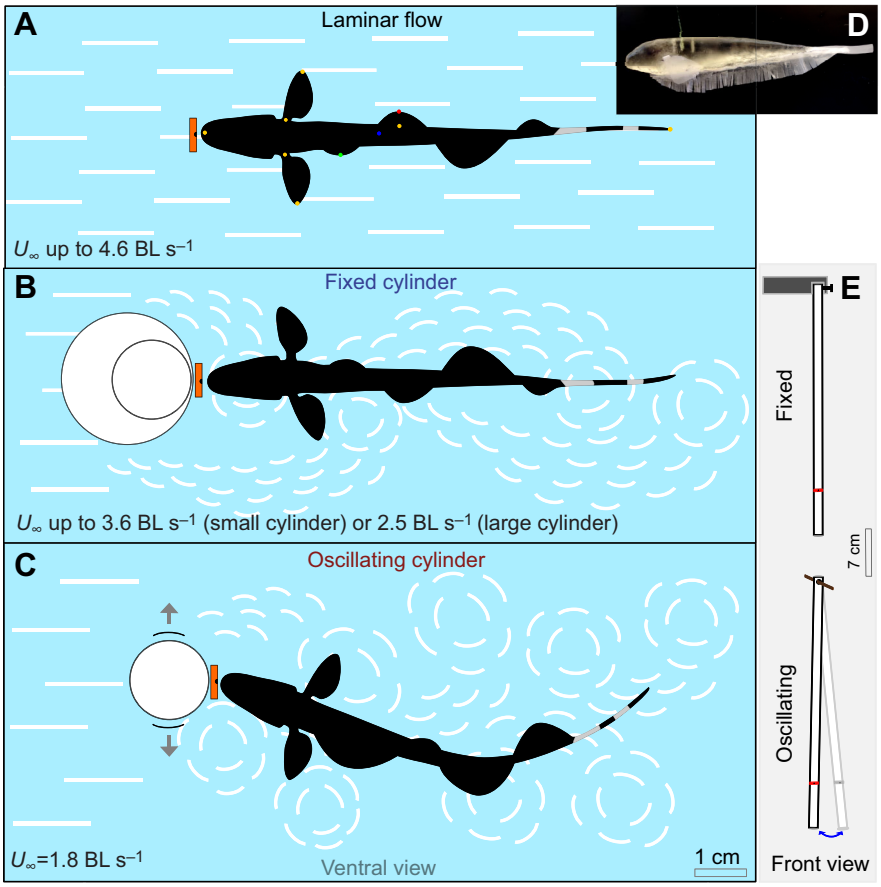

Fig. 1. Set-up showing a knifefish swimming and feeding in varied flow conditions. (A) Fish in laminar conditions at flow speeds up to 4.6 BL s^{-1}. (B) Fish swimming in the wake of a fixed cylinder (cylinder sizes: 1.6 and 2.6 cm) at varied flow speeds. (C) Fish swimming in the wake of a free oscillating cylinder at a flow speed of 1.8 BL s^{-1}. (D) Three-dimensional printed model of a knifefish. (E) Front view of a fixed (top) and an oscillating cylinder (bottom). See Fig. S3 for details of digitized points (colored dots) used for calculating kinematic variables.

introduced in the water flume. We filmed in ventral view each flow treatment with a camera filming at 300 frames s^{-1} (Fastec HiSpec 4). Using paired frames from the recorded video sequences, we calculated velocity fields and/or the vorticity fields for each flow conditions using PIVlab (Thielicke and Stamhuis, 2014; http://william.thielicke.org/PIVlab). An interrogation window from 64 to 32 pixels^2, excluding those vectors with standard deviation greater than 5, was used. The vertical offset of the horizontal laser sheet from the feeder was ∼1 cm.

To understand the role of the ribbon fin in three flow conditions (laminar, periodic vortex shedding and irregular vortex shedding), we performed particle image velocimetry (PIV) analysis as described above using only one individual. The fish was trained for 3 days to swim and feed in the dark, with the water seeded with particles and with the laser turned on at the lowest intensity. The laser sheet illuminated the area just below the feeder, and consequently, during filming, the laser sheet illuminated one side of the ribbon fin. A mirror was used to illuminate the other side. Only sequences where the entire length of the ribbon fin was illuminated by laser sheet were used. Thus, we characterized the vorticity of the wake produced by the ribbon fin of the swimming fish in laminar flow, downstream of a small fixed cylinder, and in the wake produced by an oscillating cylinder at a flow speed of 1.8 BL s^{-1}.

Reynolds number was calculated in two ways: for the body ($Re_b=U_\infty l_{body}/\nu$) and for the cylinder ($Re_{cyl}=U_\infty D_{cyl}/\nu$), where U_∞ is the flow speed, l_{body} is the body size, D_{cyl} is the cylinder diameter and ν is the kinematic viscosity of water (1×10^{-6} m^2 s^{-1}). The Strouhal number regarding the ribbon fin was calculated as $St=n_{RF}L_{RF}/U_\infty$, where n_{RF} is the ribbon fin frequency and L_{RF} is the stroke amplitude of the ribbon fin in cm. Drag force produced by ghost knifefish (F_{drag}) was estimated from the measurements taken at different pitch angles (β_b) and average flow speeds (U_f) by MacIver et al. (2010), $F_{drag}=(3.04\times10^{-3}+\beta_b\ 8.27\times10^{-2})U_f$. A previous study indicated that drag force tested using a 3D fish model at low flow speeds is similar between backward and forward swimming in black ghost knifefish (Shirgaonkar et al., 2008). Thus, power (P_{thrust}) was calculated multiplying F_{drag} by U_f. Notice that U_f corresponds to the average flow speed in the re-circulation zone of the vortex wake U_w and for the laminar conditions it corresponds to U_∞ (see Table 1). Turbulence intensity (I_t) was calculated as the ratio between the root mean square of velocity fluctuations and the mean velocity in all flow conditions at 1.8 BL s^{-1} using the velocity fields from the PIV analysis (Fig. S4).

Fish model versus oscillating cylinder

Passive movements produced by the wake of a fixed and oscillating cylinder were also investigated using a 3D printed knifefish model (Fig. 1). The model was reconstructed using 50 pictures in different orientations of a naturally deceased knifefish specimen. Fish skin was colored with watercolors for better reconstruction. We used the photogrammetry software Meshroom (https://alicevision.org/#meshroom) for the 3D fish reconstruction. MeshMixer (http://www.meshmixer.com/download.html) was used to correct and import a solid object to the 3D printer (Formlabs® Form 3). We used flexible clear resin to print the model, which had a length of 9 cm. To see passive movements of the fins, we used mesh fabric to mimic a ribbon fin (6.5×0.5 cm), pectoral fins (1.3 cm) and the tail (1 cm length). We made vertical cuts along the artificial ribbon fin (∼1 mm each) to allow passive movements of each element in the flow. Artificial fins were glued to the model using Loctite. Because

Table 1. Kinematics and flow data of knifefish swimming in varied flow conditions

	Flow															
Parameter	Laminar									Small cylinder				Large cylinder		Oscillating cylinder
N	7	7	7	7	7	7	7	6	2	7	7	7	7	7	7	7
U_∞ BL s^{-1} (cm s^{-1})	−1.4±12	1.4±12	1.8±15	2.5±21	3±26	3.6±31	3.9±33	4.3±37	4.6±39	1.8±15	2.5±21	3±26	3.6±31	1.8±15	2.5±21	1.8±15
β_b (deg)	10±5	13±3	0±3	−2±4	−3±3	−5±3	−6±2	−6±2	−11±24	9±7	−4±7	−4±11	−11±10	0±9	−12±10	−1±12
Ψ_b (deg)	8±3	7±2	5±2	6±2	7±3	7±1	7±2	6±3	7±32	17±3	11±3	14±6	14±6	18±6	15±8	21±3
γ_b (deg)	6±4	4±2	4±2	3±1	4±1	2±1	4±2	2±2	3±11	6±2	5±3	8±3	10±3	13±3	12±4	23±4
n_{RF} (Hz)	4±1	4±0	5±1	6±1	7±1	8±1	9±1	10±1	10±6	3±1	3±1	2±1	2±1	2±1	3±0	2±1
Φ_{RF} (deg)	118±20	113±15	107±18	112±7	117±10	110±20	108±11	106±8	100±110	23±12	26±10	32±15	31±9	42±11	37±12	57±8
n_{PF} (Hz)	4±1	4±1	4±1	5±2	5±1	5±2	6±2	5±1	3±3	5±1	5±1	5±1	5±1	4±1	5±1	5±0
Φ_{PF} (deg)	17±8	12±6	6±3	7±3	11±6	14±7	9±4	11±5	8±42	32±9	50±12	61±9	60±10	41±14	51±18	68±8
δ_{PF} (rad)×10^2	21±7	5±3	5±3	6±2	5±2	5±2	7±2	5±3	6±25	14±3	17±5	20±4	25±9	19±4	22±7	19±4
χ_b (deg)	13±6	5±2	5±1	4±2	6±2	5±1	7±2	7±3	6±23	16±6	15±5	19±3	17±5	21±5	27±10	44±9
L_{RF} (cm)	1±0	1±0	1±0	1±0	1±0	1±0	1±0	1±0	1±1	1±0	1±0	1±0	1±0	1±0	1±0	2±1
λ_{RF} (cm)	3±1	3±0	3±0	3±0	3±0	3±0	3±0	3±0	3±0	3±1	3±1	5±1	5±2	5±2	4±2	14±7
V_{RF} (cm s^{-1})	11±2	12±1	13±1	18±1	20±1	23±1	24±1	27±2	26±19	8±3	8±1	10±2	11±3	10±1	10±3	26±3
$V_{RF,max}$ (cm s^{-1})	13±3	13±2	15±1	20±2	22±2	27±3	28±2	33±2	35±61	11±5	11±2	13±3	13±4	12±2	12±4	37±5
a_{RF} (cm s^{-2})	46±24	35±20	45±23	86±26	103±36	164±20	183±36	210±23	226±154	81±42	76±26	103±37	121±54	81±31	89±19	483±80
Re_b ×10^3	10	10	13	18	22	26	28	31	34	13	18	21	26	13	18	13
Re_{cyl} ×10^3	–	–	–	–	–	–	–	–	–	2.5	3.3	4.1	4.9	4	5.5	2.4
St_{RF}	0.3±0.1	0.3±0	0.3±0	0.3±0	0.3±0	0.2±0	0.2±0	0.2±0	0.2±0	0.1±0.1	0.1±0	0.1±0	0.1±0	0.1±0	0.1±0	0.2±0.1
U_w (cm s^{-1})	–	–	–	–	–	–	–	–	–	2	4	5	10	2	4	8
F_{drag} (mN)*	1.6±0.2	1.7±0.1	1.9±0.2	3.4±0.6	4.8±0.6	6.3±1	7±0.6	8.5±1	7.7±11.3	0±0	0.1±0	0.2±0.1	0.5±0.3	0±0	0.1±0	0.7±0.4
P_{thrust} (mW)× 10^{-1}*	1.9±0.3	2.1±0.2	3±0.3	7.3±1.2	12.3±1.5	19.3±2.9	23.3±2	31±3.5	30.1±44.3	0.1±0	0.2±0.1	0.4±0.2	1.6±1	0.1±0	0.1±0.1	0.9±0.4

*F_{drag} and P_{thrust} were calculated using data from MacIver et al. (2010).

Columns show the sample size *N*, flow speed U_∞, pitch β_b, roll Ψ_b, yaw γ_b, ribbon fin wave frequency n_{RF}, ribbon fin wave amplitude Φ_{RF}, pectoral fin stroke frequency n_{PF}, pectoral fin stroke amplitude Φ_{PF}, pectoral fin asymmetry δ_{PF}, body bending χ_b, stroke amplitude of the ribbon fin L_{RF}, ribbon fin wave length λ_{RF}, ribbon fin wave speed V_{RF}, ribbon fin wave acceleration a_{RF}, Reynolds numbers (Re_b and Re_{cyl}), cylinder wake velocity U_w, Strouhal number St_{RF}, drag force F_{drag}, and power P_{thrust}. Data are means±95% confidence intervals. For details, see Materials and Methods.

Journal of Experimental Biology (2021) 224, jeb238808. doi:10.1242/jeb.238808

the fish model was negatively buoyant, it was suspended from a hook using flexible thin thread attached to a single point at its dorsum, which allowed it to remain fixed in position in the vertical plane, but permitted passive movement in the horizontal plane in response to flow. It is important to note that pitch angle, yaw and roll could also change passively on the model in response to flow. We filmed the fish model in laminar flow, close to the fixed cylinder and close to the oscillating cylinder at ∼2.5 BL s^{-1}. Also, for the oscillating cylinder, we placed the model at different distances downstream.

Statistical analysis

To understand how kinematics change with flow speed in laminar conditions, we performed a linear regression analysis for all measured variables. Repeated-measures ANOVA or a Friedman test was used to compare fish kinematics while swimming at 1.8 BL s^{-1} in laminar conditions, behind a large and a small fixed cylinder, and behind the oscillating cylinder. The effects on swimming performance due to cylinder size (large versus small) and flow speed (1.8 versus 2.5 BL s^{-1}) were analyzed using a two-way repeated-measures ANOVA for each kinematic variable measured. Paired *t*-tests or Wilcoxon signed-rank tests were used to compare fish swimming kinematics between laminar conditions and behind the wake produced by the small cylinder (grouping data from 1.8 to 3.6 BL s^{-1}). Similarly, we used paired *t*-tests or Wilcoxon signed-rank tests to compare kinematics between backward and forward swimming at 1.4 BL s^{-1}. Data transformation, $f(x)=\log(x)$ or $f(x)=x^p$, was applied to variables to fulfill assumptions of parametric tests when required. We used Tukey's or non-parametric pairwise comparison as *post hoc* tests when required. All data analyses were performed in R V3.6.1 (https://www.r-project.org/). Mauchly's test was performed to evaluate sphericity assumptions in repeated-measures ANOVAs. The libraries car, stats, agricolae and lsmeans were used for statistical analysis.

RESULTS

Flow conditions

Velocity fields for all laminar and unsteady flow conditions used during the experiments are shown in Fig. 2 and Figs S1 and S2. The wake produced by both fixed cylinders corresponds to a typical von Kármán vortex street at *Re* of ∼10^3–10^4. The mean flow speed U_w in the re-circulation zone for the fixed cylinders was 20–30% of the flow speed U_∞, and had an upstream direction (Fig. 2, Table 1, Fig. S2). In contrast, the wake produced by the oscillating cylinder (oscillating frequency ∼1 Hz) was irregular, with a pair of counter rotating vortices shedding laterally during each half oscillating cycle (Fig. 2). For this case, U_w was ∼50% of U_∞. The mean flow direction behind the oscillating cylinder was also upstream. Average flow velocity downstream U_w increased with cylinder size and speed (Table 1). At 1.8 BL s^{-1}, we found that U_w was largest for the oscillating cylinder in comparison with fixed cylinders. In agreement, turbulence intensities I_t for all flow conditions at 1.8 BL s^{-1} were as follows: laminar ∼2%, small cylinder 18%, large cylinder 24% and oscillating cylinder 29%.

Laminar conditions

During laminar flow, knifefish ribbon fin wave speed ($V_{RR}=5.1U_\infty+4.6$, $R^2=0.95$, $P<0.001$), acceleration ($a_{RF}=62.6U_\infty-65.4$, $R^2=0.84$, $P<0.001$) and frequency ($n_{RF}=1.8U_\infty+1.6$, $R^2=0.87$, $P<0.001$) all increased with flow speed (Fig. 3, Table S1). In contrast, fish demonstrated a significantly more head-up body orientation (pitch $\beta_b=-5.4U_\infty+14.3$, $R^2=0.6$, $P<0.001$) at higher flow speeds. The effect of speed on other kinematic variables was too small relative to the noise to infer direction (Table 1).

In contrast, fish swimming backwards showed significantly increased body bending χ_b ($t_6=-3.1$, $P<0.05$), pectoral fin asymmetry δ_{PF} ($t_6=-3.8$, $P<0.01$) and stroke amplitude of the ribbon fin L_{RF} ($t_6=-4.6$, $P<0.01$) in comparison with forward swimming at the same speed (Fig. 4). We found no evidence of significant differences between backward and forward swimming for other kinematic variables measured ($P>0.5$ for all contrasts) (Table 1).

Laminar versus small cylinder

Fish swimming downstream of the small cylinder presented significantly larger pectoral fin stroke amplitude Φ_{PF} (Wilcoxon test, $V=06$, $P<0.001$), body bending χ_b ($t_{27}=11.6$, $P<0.001$), pectoral fin asymmetry δ_{PF} ($t_6=10.4$, $P<0.001$), roll Ψ_b ($t_{27}=6$, $P<0.001$) and yaw γ_b ($t_{27}=5.6$, $P<0.001$) in comparison with laminar flow conditions. In contrast, fish swimming downstream of the small cylinder showed lower ribbon fin wave speed V_{RF} ($t_{27}=-13.3$, $P<0.001$), wave amplitude Φ_{RF} (Wilcoxon test, $V=0$, $P<0.001$), stroke amplitude L_{RF} ($t_{27}=-3.9$, $P<0.001$) and frequency n_{RF} (Wilcoxon test, $V=0$, $P<0.001$) (Table 1) in comparison with control conditions.

Cylinder size versus flow speed

Two-way repeated-measures ANOVAs indicated a main effect between cylinder sizes on ribbon fin wave frequency n_{RF} ($F_{1,6}=6.9$, $P=0.039$), stroke amplitude Φ_{RF} ($F_{1,6}=13.1$, $P=0.01$), body bending χ_b ($F_{1,6}=15.1$, $P<0.01$), stroke amplitude L_{RF} ($F_{1,6}=13.1$, $P=0.01$) and yaw γ_b ($F_{1,6}=350$, $P<0.001$). Also, there was a significant main effect between speeds on pitch β_b ($F_{1,6}=20.7$, $P<0.01$). There was no evidence that the association between cylinder size and flow speed varied in any kinematic variables ($P>0.05$) (Table 1).

Laminar, fixed cylinders and oscillating cylinder

Comparisons among fish swimming in laminar flow, small fixed cylinder, large fixed cylinder and oscillating small cylinder at 1.8 BL s^{-1} indicate significant differences in n_{RF} ($F_{1,3}=8.5$, $P<0.01$), Φ_{RF} ($F_{1,3}=49.9$, $P<0.001$), V_{RF} ($\chi^2_{1,3}=18.9$, $P<0.001$), a_{RF} ($\chi^2_{1,3}=14.1$, $P<0.01$), L_{RF} ($F_{1,3}=35.7$, $P<0.001$), Φ_{PF} ($F_{1,3}=57.9$, $P<0.001$), δ_{PF} ($F_{1,3}=24.9$, $P<0.001$), χ_b ($F_{1,3}=70.6$, $P<0.001$), Ψ_b ($F_{1,3}=18.5$, $P<0.001$) and γ_b ($F_{1,3}=29.3$, $P<0.001$). In contrast, no evidence of significant differences among treatments were found in n_{PF} ($F_{1,3}=2.2$, $P>0.05$) or β_b ($F_{1,3}=1.3$, $P>0.05$) (Figs 5–7).

Post hoc tests revealed that fish in laminar flows presented the largest ribbon fin frequency n_{RF}, amplitude Φ_{RF} and stroke amplitude L_{RF} when compared with other conditions (for all comparisons, $P<0.05$). Ribbon fin wave speed V_{RF} in laminar conditions was higher than in both fixed cylinder conditions. In contrast, fish in laminar conditions had the smallest wave acceleration a_{RF}, pectoral fin amplitude n_{PF}, pectoral fin asymmetry δ_{PF}, roll Ψ_b and body bending χ_b than across the three other conditions ($P<0.05$). Similarly, yaw γ in laminar flow was significantly smaller than in the large fixed and oscillating cylinder conditions ($P<0.05$). Fish swimming downstream of the oscillating cylinder had the highest a_{RR}, V_{RF}, Φ_{PF}, γ_b and χ_b. Similarly, individuals demonstrated significantly larger ribbon fin amplitude Φ_{RF} and δ_{PF} for the oscillating cylinder when compared with the small fixed cylinder (all $P<0.05$), but L_{RF} was significantly higher for both fixed cylinder conditions (all $P<0.05$). Fish downstream of

Journal of Experimental Biology (2021) 224, jeb238808. doi:10.1242/jeb.238808

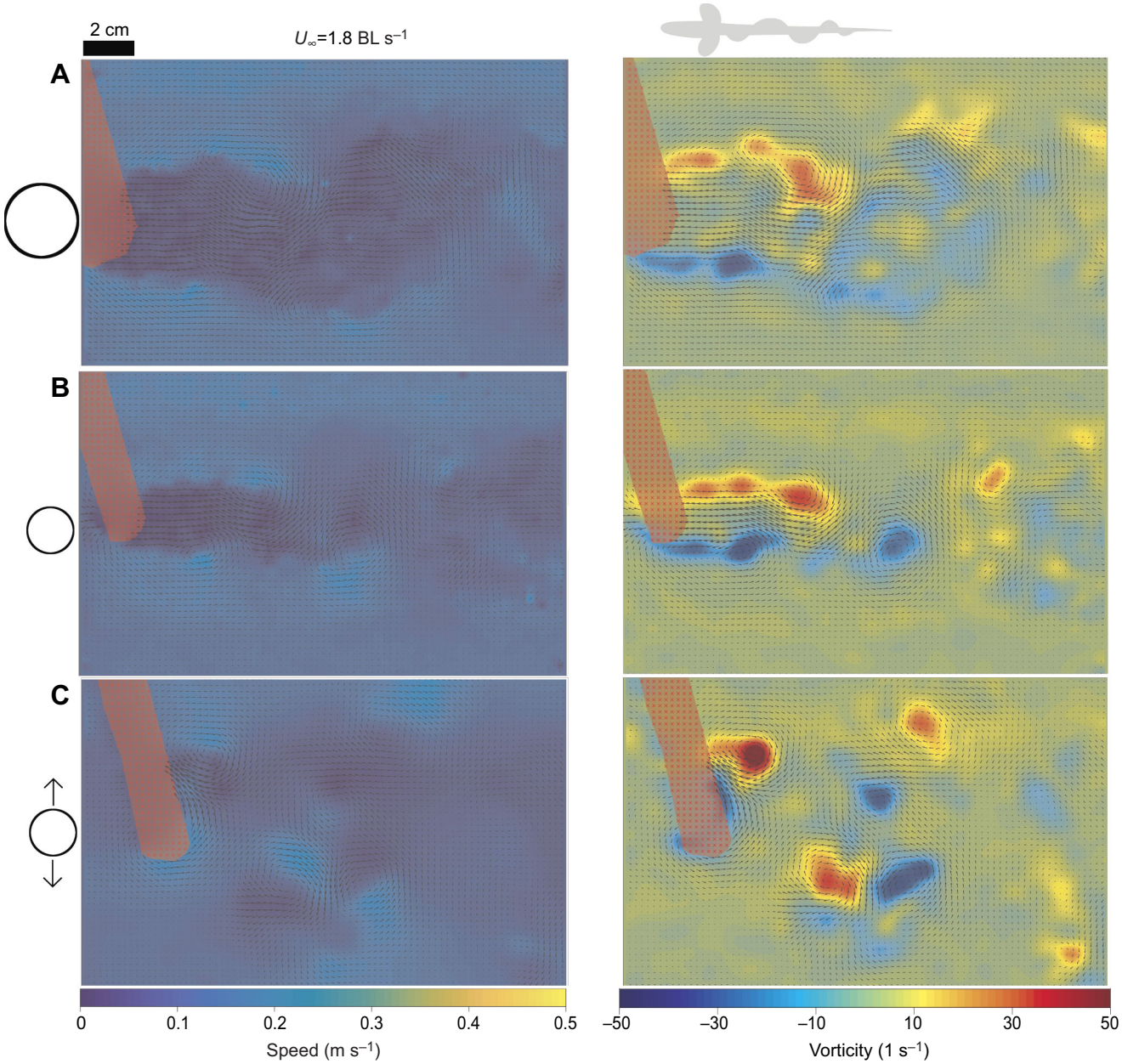

Fig. 2. Example of velocity and vorticity fields of the wake produced by the different cylinders at a flow speed of 1.8 BL s^{-1}. (A) Large fixed cylinder, (B) small fixed cylinder and (C) oscillating cylinder. See Figs S1 and S2 for all other flow conditions.

the large fixed cylinder at 1.8 BL s^{-1} had significantly higher δ_{PF}, Φ_{RF}, γ_b and L_{RF} than fish downstream of the small fixed cylinder. Power (P_{thrust}) in the small fixed cylinder and the oscillating cylinder was 3% and 30%, respectively, when compared with the power required during laminar flow (see Table 1).

Fish model

The fish model placed at different distances in the re-circulation zone of the small fixed cylinder first moved toward and then remained attached to the cylinder while keeping a fixed horizontal body orientation (see Movie 1). Ribbon and pectoral fins exhibited irregular oscillations. In contrast, the model placed close to an oscillating cylinder (<1 cylinder diameter downstream) showed body oscillations that were out of phase with the cylinder oscillations (Movie 1). Body orientation (yaw and roll), as well as the pectoral fins and the ribbon fins, were affected during each cylinder's oscillation cycle. However, when the fish was placed approximately one cylinder diameter downstream in the wake of the oscillating cylinder, it started moving in phase with the cylinder. Moreover, the fish model demonstrated small disruptions in body orientation and fin movements than when located <1 cylinder diameter downstream. These results suggest that, when located immediately downstream of an oscillating cylinder, a knifefish will need to actively overcome the out-of-phase motion resulting from the wake of an oscillating cylinder; while downstream of a fixed cylinder, the fish can remain stationary with minimal effort.

PIV on ribbon fin

Using DPIV, we verified that the ribbon fin produces a vortex street wake in both laminar flow and behind an oscillating cylinder, but

Journal of Experimental Biology (2021) 224, jeb238808. doi:10.1242/jeb.238808

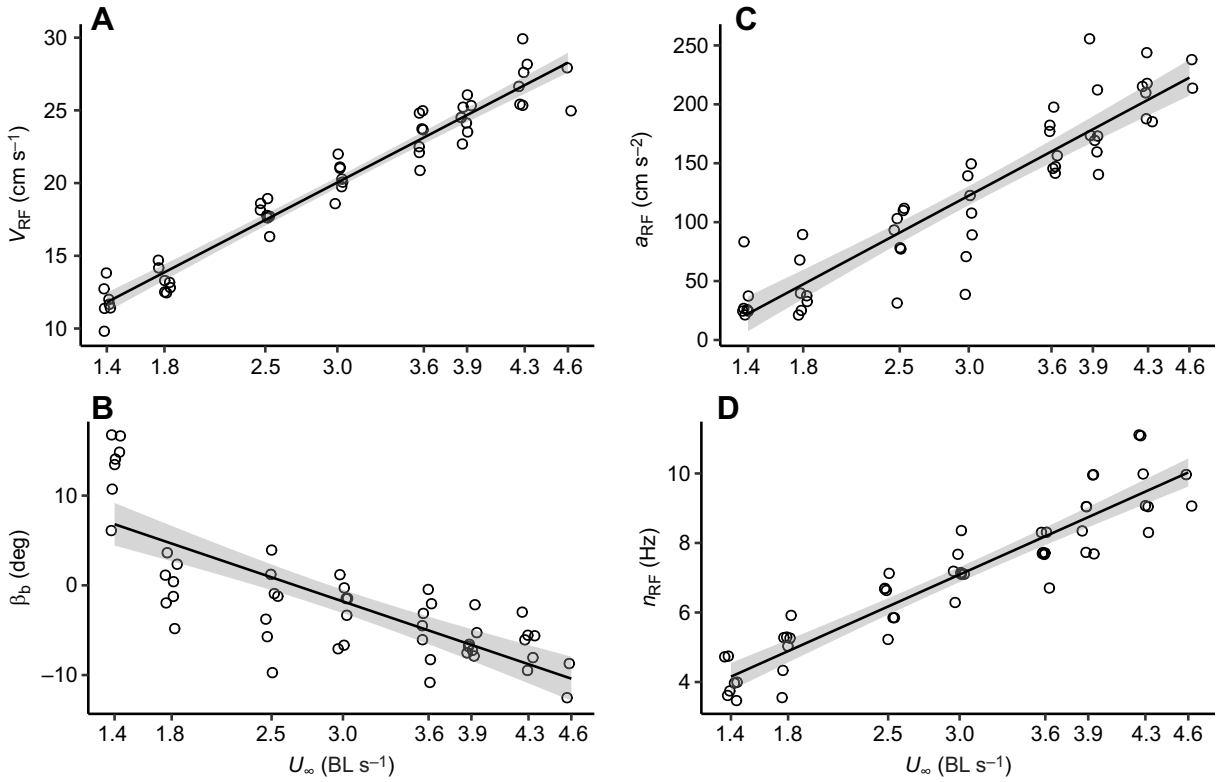

Fig. 3. Linear fits of the ribbon fin parameters and body pitch versus flow speed U_∞. (A) Wave speed (V_{RF}=5.1U_∞+4.6, R^2=0.95, P<<0.001), (B) body pitch (β_b=−5.4U_∞+14.3, R^2=0.6, P<<0.001), (C) ribbon fin wave acceleration (a_{RF}=62.6U_∞–65.4, R^2=0.84, P<<0.001) and (D) ribbon fin wave frequency (n_{RF}=1.8U_∞+1.6, R^2=0.87, P<<0.001). Sample size was n=7 for U_∞ from −1.4 to 3.9 BL s^{-1}, n=6 for U_∞=4.3 and n=2 for U_∞=4.6. The position-jitter function in R was used to show overlapping data.

not when the fish is swimming downstream of a fixed cylinder. In a laminar flow (1.8 BL s^{-1}), the ribbon fin of a knifefish produces a continuous wake of counter-oscillating eddies (Movie 1). In contrast, the ribbon fin of a knifefish downstream from a fixed cylinder is moving passively with the cylinder's wake and there is no evidence of active vortical structure. Further, the ribbon fin of a knifefish swimming downstream from an oscillating cylinder is actively generating a vortex street similar to that found in laminar flow, which is only amplified during turning and acceleration in an effort to reach the feeder (Fig. 8, Movie 1).

DISCUSSION

Gymnotiforms are well known for their ability to swim through complex structured and dynamically changing environments characteristic of their natural habitat, such as the Amazon River. In such conditions, in which it is difficult to hold station, maneuver or provide adequate thrust production, it becomes necessary to partition forces generated by the different control surfaces such as paired and median fins as well as body movements. Here, we experimentally demonstrated that the black ghost knifefish uses alternate gaits depending on the dynamics of the flow perturbation. Knifefish swimming in laminar flow is dominated by ribbon fin movements while keeping the body rigid. In contrast, knifefish located downstream of a fixed cylinder maintain position using a gait driven by asymmetrical pectoral fin strokes coupled with body bending and marked changes in body orientation. Knifefish swimming downstream of a passively oscillating cylinder use a combination of ribbon and pectoral fin movements and body bending to overcome the out-of-phase displacements induced by the oscillatory vortex wake. The latter may have important implications in predator–prey interactions, or even collective locomotion, as the wake produced by an organism experiencing an oscillatory pattern can influence the trajectory or gait of another organism located downstream or in proximity.

Knifefish swimming performance has been extensively investigated in still water or laminar flows generated in a swim tunnel (Blake, 1983; Ruiz-Torres et al., 2013; Youngerman et al., 2014). These studies have focused on the role of the ribbon fin in swimming in any direction or even staying still in mid water. Furthermore, a recent study suggested that fish using the ribbon fin for thrust production have sprint speeds and energetic costs similar to those of subcarangiform swimmers that use body-caudal fin undulations (Whitlow et al., 2019). Here, we found that wave frequency n_{RF} and wave speed V_{RF} of the ribbon fin increase with flow speed up to 5 BL s^{-1}, which agrees with previous work of knifefish swimming forward up to ∼2 BL s^{-1} (Ruiz-Torres et al., 2013). Furthermore, at maximal flow speed individuals showed n_{RF} and V_{RF} values up to 12 Hz and 43 cm s^{-1}, respectively, which may be the upper limit of the ribbon fin performance (Fig. 3). One intriguing result is that the average wave acceleration along the ribbon fin is not zero, but increases with flow speed from 5% to 20% the acceleration of gravity (Table 1). This indicates that the wave velocity along the ribbon fin is not uniform, at least in the region where the measurement was made. Furthermore, this could suggest that the vortex wake produced at the leading edge is contributing to fin ray movements and thus the wave pattern in the caudal region of the ribbon fin. This also may suggest that ribbon fin rays are not all fully active, but only those at the anterior. This aligns with the

Journal of Experimental Biology (2021) 224, jeb238808. doi:10.1242/jeb.238808

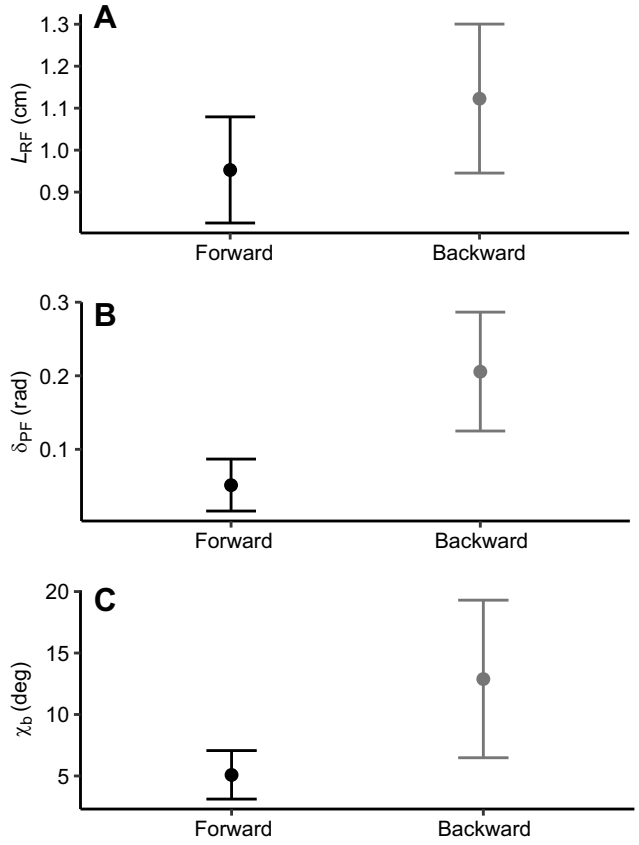

Fig. 4. Backward versus forward swimming at 1.4 BL s^{-1}. (A) Stroke amplitude of the ribbon fin L_{RF} in cm, (B) pectoral fin asymmetry δ_{PF} and (C) body bending χ_b. Data are means±1 s.d. (n=7).

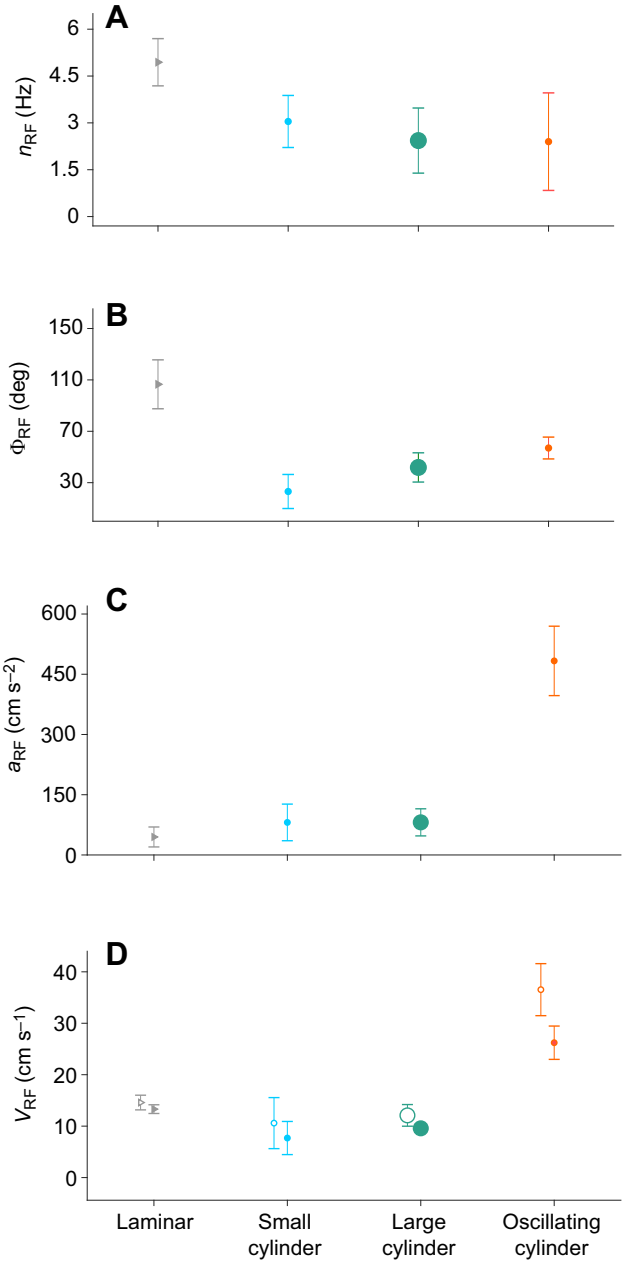

Fig. 5. Ribbon fin kinematics of knifefish swimming in laminar conditions (gray symbols) and in the wake of the small fixed cylinder (blue symbols), the large fixed cylinder (green symbols) and the oscillating cylinder (orange symbols). (A) Wave frequency n_{RF}, (B) wave stroke amplitude Φ_{RF}, (C) wave acceleration a_{RF} and (D) maximal (open symbols) and average (filled symbols) wave speed V_{RF}. Data are means±1 s.d. (n=7).

discovery that flapping foils actuated only at the anterior move in a regular undulatory pattern, producing a wake similar to that of swimming eels (Lauder et al., 2011). Furthermore, results on head-up posture with increasing flume velocity may be a consequence of ribbon fin acceleration and pectoral fin lift. Future investigation of this possibility would be supported by sampling more points along the ribbon fin, and will further elucidate ribbon fin dynamics in thrust production.

Backward swimming is commonly used by knifefish during prey capture (Lannoo and Lannoo, 1993) or to rapidly extract themselves from narrow spaces. Prior work has demonstrated that black ghost knifefish use the ribbon fin to propel themselves backwards by reversing the ribbon fin wave, from tail to head (Youngerman et al., 2014). However, the role of the pectoral fins or body bending in knifefish swimming has not been investigated. We found that knifefish swimming backwards must compensate for unsteady body orientation using asymmetrical strokes of the pectoral fins. Furthermore, knifefish swimming in reverse could not maintain a stable position above 2 BL s^{-1}. The unstable body position during backwards swimming could be a consequence of a caudal region and ribbon fin that is flat rather than streamlined. Thus, any small displacement in yaw will generate drag forcing, tending to amplify yaw, which may explain why at low flow speeds knifefish are indeed able to maintain position using asymmetrical movements of the pectoral fins.

Fish locomotion research in unsteady flows has been dominated by subcarangiform swimmers (see Liao, 2007 for review). For example, Liao et al. (2003a,b) demonstrated that trout swimming in Kármán vortices were able to reduce muscle activity and passively hold position downstream by matching body undulations to vortex shedding oscillations. However, this so-called Kármán gait can easily be disrupted by flow disturbances and is entirely dependent on downstream position, flow speed, body size, body kinematics and wake dynamics of the cylinder (Akanyeti and Liao, 2013; Yuan and Hu, 2017). Similarly, trout can use entraining to reduce swimming costs, which results from holding position close to the cylinder by tilting the body at one side of the vortex shedding (Przybilla et al., 2010). Entraining can also be easily disrupted, and fish commonly show erratic pectoral fin and body movements

Journal of Experimental Biology (2021) 224, jeb238808. doi:10.1242/jeb.238808

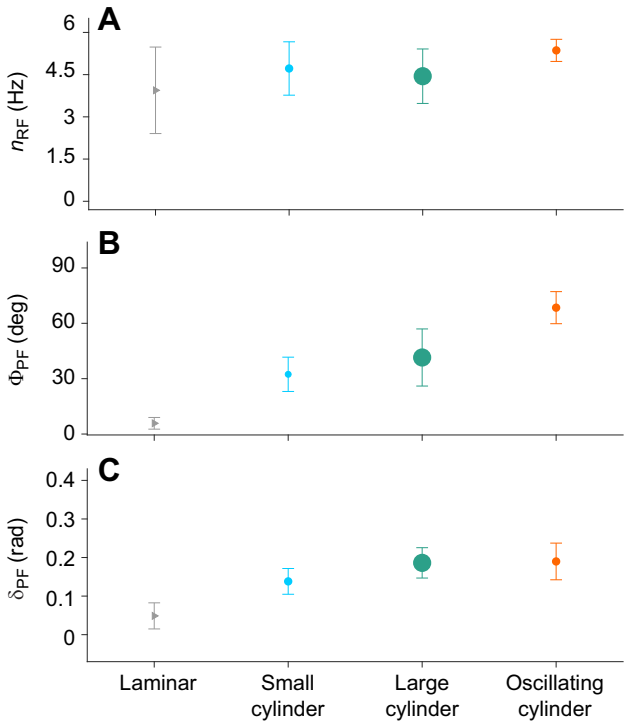

Fig. 6. Pectoral fin kinematics of knifefish swimming in laminar conditions (gray symbols) and in the wake of the small fixed cylinder (blue symbols), the large fixed cylinder (green symbols) and the oscillating cylinder (orange symbols). (A) Stroke frequency n_{PF}, (B) stroke amplitude Φ_{PF} and (C) pectoral fin asymmetry δ_{PF}. Data are means±1 s.d. (n=7).

alternated with short periods of non-movement. Flying animals moving in a Kármán vortex street are also dependent on substantial lift and thrust forces to remain airborne. Thus, fliers demonstrate dramatic changes in wing and body kinematics that are dependent on vortex size and downstream distance (see Ortega-Jimenez et al., 2016). Here, we demonstrated that knifefish swimming in the re-circulation zone downstream of a fixed cylinder, irrespective of flow speed, actively use their pectoral fins with asymmetrical movements, but do not use the ribbon fin. As a result, we found that the ribbon fin stroke amplitude was much smaller in comparison with fish swimming in laminar flows. Also, knifefish that are station holding downstream of large cylinders are characterized by marked changes in body orientation and body bending. On average, the flow direction in the re-circulation zone of a fixed cylinder is directed upstream, necessitating backwards swimming in the knifefish in order to compensate for unsteady incoming vortices and maintain position. As discussed above, swimming backwards is challenging, but knifefish employ the pectoral fins to mitigate unstable body position. Power estimates (P_{thrust}=F_{drag}×U_f; MacIver et al., 2010) indicate that knifefish swimming behind a cylinder require only ∼3% of the power required to overcome drag force per unit of time in laminar conditions at the same flow speed. Reduction in swimming costs are also supported by our experiments using a printed fish model and PIV flow patterns behind a fixed cylinder, and passive movements of the ribbon fin. However, our power estimates assume that the body and ribbon fin is maintained in a rigid configuration (MacIver et al., 2010). Thus, a more accurate estimate would include the cost associated with pectoral fin movements, body orientation and body bending. Future respirometry measurements and investigations of muscle activity on knifefish would help to provide a more comprehensive understanding of the swimming cost in unsteady flows. It is important to notice that knifefish morphology and swimming mode are very different than those of salmonids; thus a direct comparison of our result with those of previous fish studies should be treated with caution.

In nature, loose and flexible natural structures, such as plants, submerged logs or rocks, exposed to flows are prone to oscillation owing to a phenomenon known as vortex-induced vibration (Williamson and Govardhan, 2004). This can be understood as a

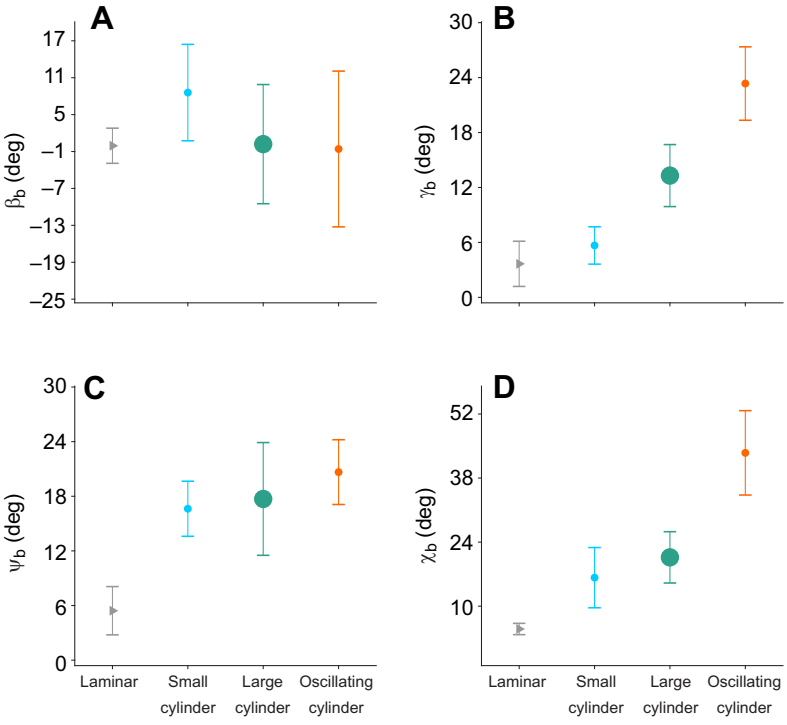

Fig. 7. Body kinematics of knifefish swimming in laminar conditions (gray symbols) and in the wake of the small fixed cylinder (blue symbols), the large fixed cylinder (green symbols) and the oscillating cylinder (orange symbols). (A) Pitch β_b, (B) yaw γ_b, (C) roll Ψ_b and (D) body bending χ_b. Data are means±1 s.d. (n=7).

Journal of Experimental Biology (2021) 224, jeb238808. doi:10.1242/jeb.238808

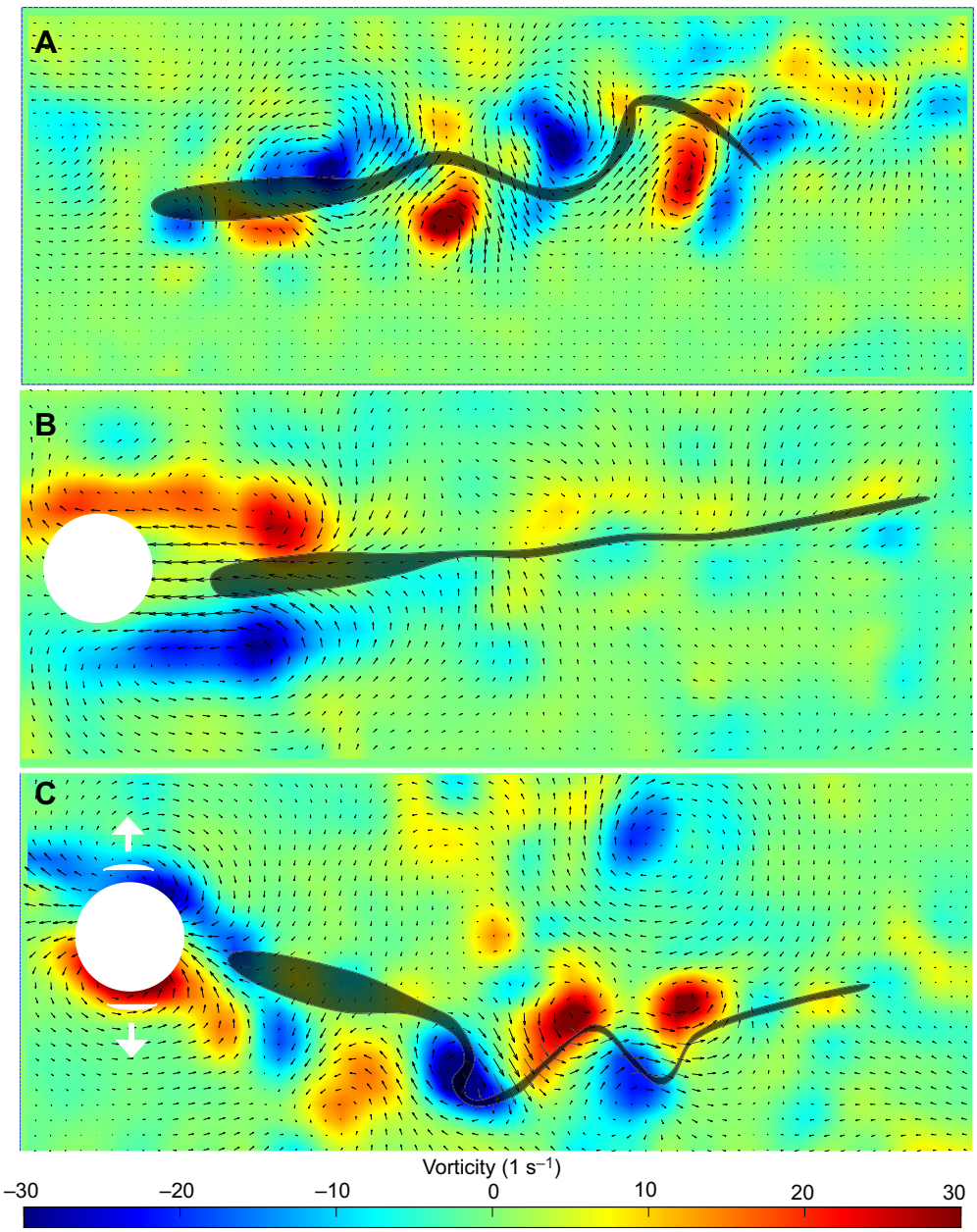

Fig. 8. Vorticity fields produced by the knifefish ribbon fin in different flow conditions. (A) Laminar, (B) behind the small, fixed cylinder and (C) behind the oscillating cylinder. For all conditions, flow speed was 1.8 BL s^{-1}. See Movie 1.

feedback system because bluff body oscillations are induced by the vortex shedding, which at the same time produce irregularities on the wake. The result is a more complex vortex pattern than those associated with fixed, bluff bodies (i.e. a Kármán vortex street). Thus, flying and swimming animals moving in such irregular wakes must respond accordingly to overcome those challenges. To our knowledge, the present study is the first to investigate swimming performance of fish moving in the vortex shedding produced by a free oscillating cylinder. We found that black ghost knifefish actively use pectoral and ribbon fins, along with body bending movements to overcome the out-of-phase oscillations induced by the irregular wake. Passive out-of-phase movements were verified in a fish model placed behind the oscillation cylinder (Movie 1). Not surprisingly, fish demonstrated large disruptions in body orientation, particularly in yaw. Furthermore, we found the highest wave speeds, wave accelerations and large wave amplitudes of the ribbon fin in knifefish swimming just downstream of an oscillating cylinder. Body bending, coupled with large ribbon fin excursions, is required in order to produce the hydrodynamic forces necessary to maintain position, especially when the cylinder changes direction. Using DPIV, we confirmed that strong vortices are formed by the ribbon fin when fish change direction. Consistently, we estimated that the power cost P_{thrust} was 10 times higher than that obtained in the fixed cylinder case. This elevated power is likely due to a higher average flow speed in the re-circulation area of the oscillating cylinder (Table 1). Thus, it is expected that knifefish moving through streams disrupted by vortex-induced vibrations will experience a higher cost for maneuvering and thrust production, than when swimming through Kármán vortex streets. It is notable that no extra momentum in the flow was introduced in the case of an oscillating cylinder. Those oscillations were free (not forced), which means that no actuators were used. Consequently, both wakes produced by fixed and oscillating cylinder were only driven by the kinetic energy of the incoming laminar flow, which is why both conditions had the same

Reynolds numbers. Further investigation would help to discover if the ribbon fin is recapturing some energy resulting from the vortex produced by the oscillating cylinder.

Another remarkable discovery was the emergence of passive movements produced by unsteady flow conditions on a printed fish model. Behind the fixed cylinder, the model moved toward the cylinder and remained attached to it. In contrast, the fish model located immediately behind the oscillating cylinder started oscillating out of phase, but when placed one cylinder distance downstream, it oscillated in phase with the cylinder. Differences in body kinematics between live fish and physical models were attributed to the model being inflexible and not bending the body as the fish does, but also the lack of active control owing to pectoral and ribbon fins. Despite these differences, passive oscillations behind an oscillating cylinder were similar in both the fish and the printed model (Movie 1).

These passive movements produced by oscillating objects may have broad biological implications. For example, parasitoid fliers such as wasps approaching prey downstream on an oscillating branch will have difficulty landing because of the passive movements generated by the branch's wake, which could present an opportunity for the prey to escape. A predator's optical flow also will be affected by the oscillations. Similarly, under certain conditions during predator–prey interaction or during intra-specific chasing of both swimmers and fliers, the leading animal can affect the path of the animal downstream by following an oscillating path. To escape, it is possible for the former to perform a sharp turn during maximal out-of-phase oscillations. In swarms and during gregarious migration, small path undulation disruptions by the leaders can grow downstream, increasing locomotion costs, as well as impacting locomotory control of the animals positioned downstream. Vortex-induced oscillation may also affect feeding performance in soft corals (Alcyonacea), as well as their predators, such as butterflyfish. Future research on those topics will greatly benefit from a deeper understanding of the effects of irregular wakes on animal interactions.

In conclusion, our results indicate that knifefish have different gaits depending of flow dynamics. In laminar flows, fish swim using predominantly the ribbon fin. In contrast, in Kármán vortex streets, knifefishes rely primarily on pectoral fin movements. In the irregular wake of a free oscillating cylinder, fish swim using their ribbon and pectoral fins, as well as body bending. In general, these results indicate that vortex-induced vibration systems present significant additional challenges to locomotor control and stability, as well as higher energy costs for swimmers and flying animals when compared with Kármán vortex streets.

Acknowledgements
We thank Sarahi Arriaga-Ramirez for her comments on an earlier version of the paper.

Competing interests
The authors declare no competing or financial interests.

Author contributions
Conceptualization: V.M.O., C.P.S.; Methodology: V.M.O.; Software: V.M.O.; Validation: V.M.O.; Formal analysis: V.M.O.; Investigation: V.M.O.; Resources: C.P.S.; Data curation: V.M.O.; Writing - original draft: V.M.O.; Writing - review & editing: V.M.O., C.P.S.; Visualization: V.M.O.; Supervision: V.M.O., C.P.S.; Project administration: C.P.S.; Funding acquisition: C.P.S.

Funding
This research was supported by funds from Kennesaw State University College of Science and Mathematics.

Data availability
The PIV and Digitization software that support the findings of this study are available at https://pivlab.blogspot.com/2017/07/pivlab-direct-download.html and http://biomech.web.unc.edu/dltdv/, respectively. Datasets have been deposited in the Dryad Digital Repository (Ortega-Jiménez et al., 2021): https://doi.org/10.5061/dryad.sqv9s4n37.

References
Akanyeti, O. and Liao, J. C. (2013). The effect of flow speed and body size on Kármán gait kinematics in rainbow trout. *J. Exp. Biol.* **216**, 3442-3449. doi:10.1242/jeb.087502

Blake, R. W. (1983). Swimming in the electric eels and knifefishes. *Can. J. Zool.* **61**, 1432-1441. doi:10.1139/z83-192

Combes, S. A. and Dudley, R. (2009). Turbulence-driven instabilities limit insect flight performance. *Proc. Natl. Acad. Sci. USA* **106**, 9105-9108. doi:10.1073/pnas.0902186106

Crampton, W. G. R. (1998). Electric signal design and habitat preferences in a species rich assemblage of gymnotiform fishes from the upper Amazon basin. *An. Acad. Bras. Ci.* **70**, 805-847.

Lannoo, M. J. and Lannoo, S. J. (1993). Why do electric fishes swim backwards? An hypothesis based on gymnotiform foraging behavior interpreted through sensory constraints. *Environ. Biol. Fishes* **36**, 157-165. doi:10.1007/BF00002795

Lauder, G. V. (2015). Fish locomotion: recent advances and new directions. *Annu. Rev. Mar. Sci.* **7**, 521-545. doi:10.1146/annurev-marine-010814-015614

Lauder, G. V., Lim, J., Shelton, R., Witt, C., Anderson, E. and Tangorra, J. L. (2011). Robotic models for studying undulatory locomotion in fishes. *Mar. Tech. Soc. J.* **45**, 41-55. doi:10.4031/MTSJ.45.4.8

Liao, J. C. (2007). A review of fish swimming mechanics and behaviour in altered flows. *Philos. Trans. R. Soc. B Biol. Sci.* **362**, 1973-1993. doi:10.1098/rstb.2007.2082

Liao, J. C., Beal, D. N., Lauder, G. V. and Triantafyllou, M. S. (2003a). Fish exploiting vortices decrease muscle activity. *Science* **302**, 1566-1569. doi:10.1126/science.1088295

Liao, J. C., Beal, D. N., Lauder, G. V. and Triantafyllou, M. S. (2003b). The Kármán gait: novel body kinematics of rainbow trout swimming in a vortex street. *J. Exp. Biol*. **206**, 1059-1073. doi:10.1242/jeb.00209

Maia, A., Sheltzer, A. P. and Tytell, E. D. (2015). Streamwise vortices destabilize swimming bluegill sunfish (*Lepomis macrochirus*). *J. Exp. Biol.* **218**, 786-792. doi:10.1242/jeb.114363

MacIver, M. A., Patankar, N. A. and Shirgaonkar, A. A. (2010). Energy–information trade-offs between movement and sensing. *PLoS Comput. Biol.* **6**, e1000769. https://doi.org/10.1371/journal.pcbi.1000769

Ortega-Jimenez, V. M., Greeter, J. S. M., Mittal, R. and Hedrick, T. L. (2013). Hawkmoth flight stability in turbulent vortex streets. *J. Exp. Biol.* **216**, 4567-4579. doi:10.1242/jeb.089672

Ortega-Jimenez, V. M., Sapir, N., Wolf, M., Variano, E. A. and Dudley, R. (2014). Into turbulent air: size-dependent effects of von Kármán vortex streets on hummingbird flight kinematics and energetics. *Proc. R. Soc. B Biol. Sci.* **281**, 20140180. doi:10.1098/rspb.2014.0180

Ortega-Jimenez, V. M., Badger, M., Wang, H. and Dudley, R. (2016). Into rude air: hummingbird flight performance in unpredictable aerial environments. *Philos. Trans. R. Soc. B Biol. Sci.* **371**, 20150387. doi:10.1098/rstb.2015.0387

Ortega-Jiménez, V. M. and Sanford, C. P. (2021). Beyond the Karman gait: knifefish swimming in periodic and irregular vortex streets. Dryad, Dataset, https://doi.org/10.5061/dryad.sqv9s4n37

Przybilla, A., Kunze, S., Rudert, A., Bleckmann, H. and Brücker, C. (2010). Entraining in trout: a behavioural and hydrodynamic analysis. *J. Exp. Biol.* **213**, 2976-2986. doi:10.1242/jeb.041632

Ruiz-Torres, R., Curet, O. M., Lauder, G. V. and MacIver, M. A. (2013). Kinematics of the ribbon fin in hovering and swimming of the electric ghost knifefish. *J. Exp. Biol.* **216**, 823-834. doi:10.1242/jeb.076471

Sefati, S., Neveln, I. D., Roth, E., Mitchell, T. R., Snyder, J. B., Maciver, M. A., Fortune, E. S. and Cowan, N. J. (2013). Mutually opposing forces during locomotion can eliminate the tradeoff between maneuverability and stability. *Proc. Natl. Acad. Sci. USA* **110**, 18798-18803. doi:10.1073/pnas.1309300110

Shirgaonkar, A. A., Curet, O. M., Patankar, N. A. and MacIver, M. A. (2008). The hydrodynamics of ribbon-fin propulsion during impulsive motion. *J. Exp. Biol.* **211**, 3490-3503. doi:10.1242/jeb.019224

Sîrbulescu, R. F., Ilieş, I. and Zupanc, G. K. H. (2009). Structural and functional regeneration after spinal cord injury in the weakly electric teleost fish, *Apteronotus leptorhynchus*. *J. Comp. Physiol. A* **195**, 699-714. doi:10.1007/s00359-009-0445-4

Steinbach, A. B. (1970). Diurnal movements and discharge characteristics of electric gymnotid fishes in the Rio Negro, Brazil. *Biol. Bull.* **138**, 200-210. doi:10.2307/1540202

Thielicke, W. and Stamhuis, E. J. (2014). PIVlab – Towards user-friendly, affordable and accurate digital particle image velocimetry in MATLAB. *J. Open Res. Soft.* **2**, e30. doi:10.5334/jors.bl

Thompson, A., Infield, D. T., Smith, A. R., Smith, G. T., Ahern, C. A. and Zakon, H. H. (2018). Rapid evolution of a voltage-gated sodium channel gene in a lineage of electric fish leads to a persistent sodium current. *PLoS Biol.* **16**, e2004892. doi:10.1371/journal.pbio.2004892

Tucker, V. A. (1972). Metabolism during flight in the laughing gull, *Larus atricilla*. *Am. J. Physiol.* **222**, 237-245. doi:10.1152/ajplegacy.1972.222.2.237

Walker, J. A. (1998). Estimating velocities and accelerations of animal locomotion: a simulation experiment comparing numerical differentiation algorithms. *J. Exp. Biol.* **201**, 981-995.

Whitlow, K. R., Santini, F. and Oufiero, C. E. (2019). Convergent evolution of locomotor morphology but not performance in gymnotiform swimmers. *J. Evol. Biol* **32**, 76-88. doi:10.1111/jeb.13399

Williamson, C. H. K. and Govardhan, R. (2004). Vortex-induced vibrations. *Annu. Rev. Fluid Mech.* **36**, 413-455. doi:10.1146/annurev.fluid.36.050802.122128

Youngerman, E. D., Flammang, B. E. and Lauder, G. V. (2014). Locomotion of free-swimming ghost knifefish: anal fin kinematics during four behaviors. *Zoology* **117**, 337-348. doi:10.1016/j.zool.2014.04.004

Yuan, H. T. and Hu, W. R. (2017). A numerical study of tadpole swimming in the wake of a d-section cylinder. *J. Hydrodyn.* **29**, 1044-1053. doi:10.1016/S1001-6058(16)60818-1

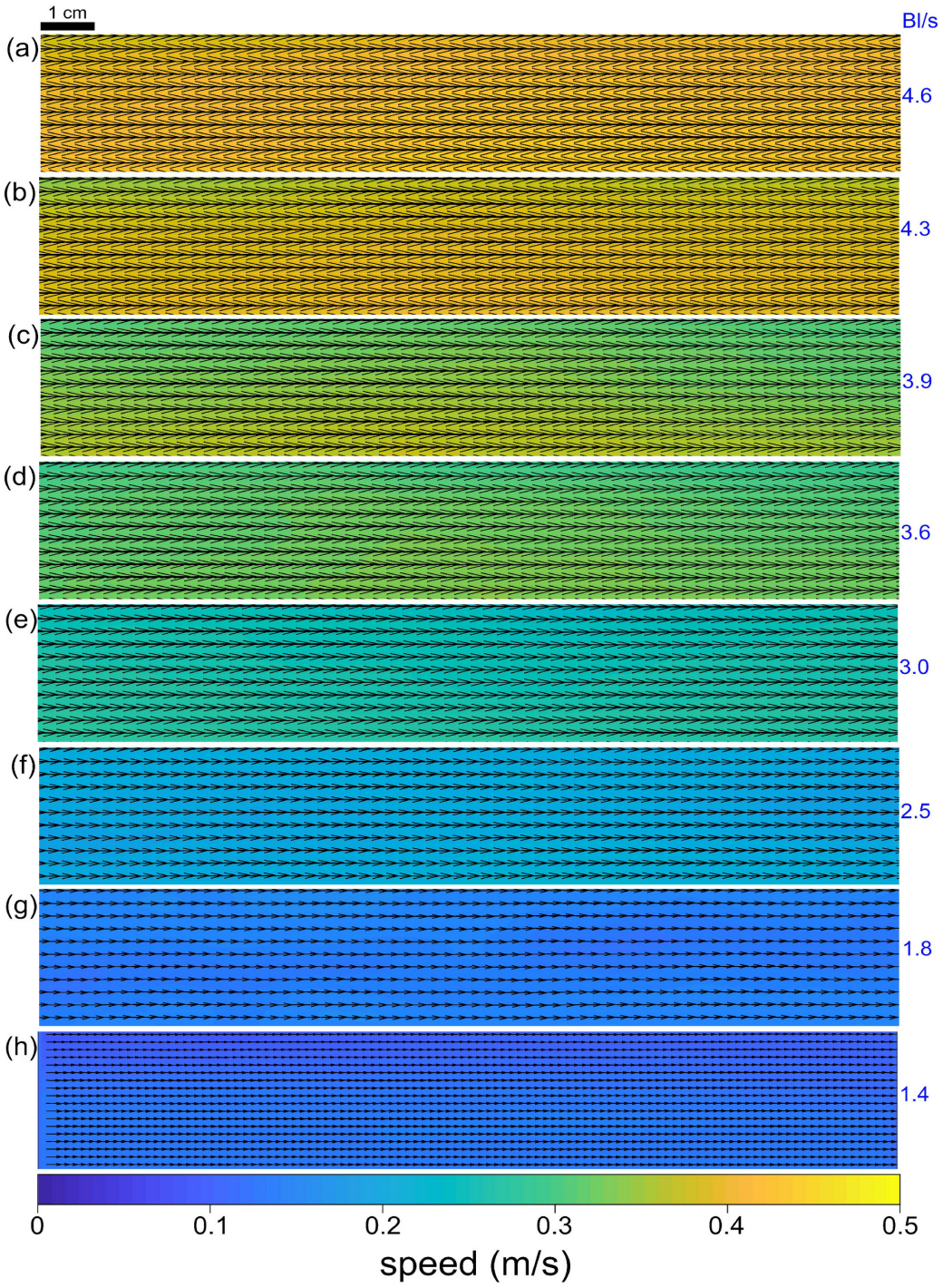

Figure S1. Velocity fields of laminar conditions.

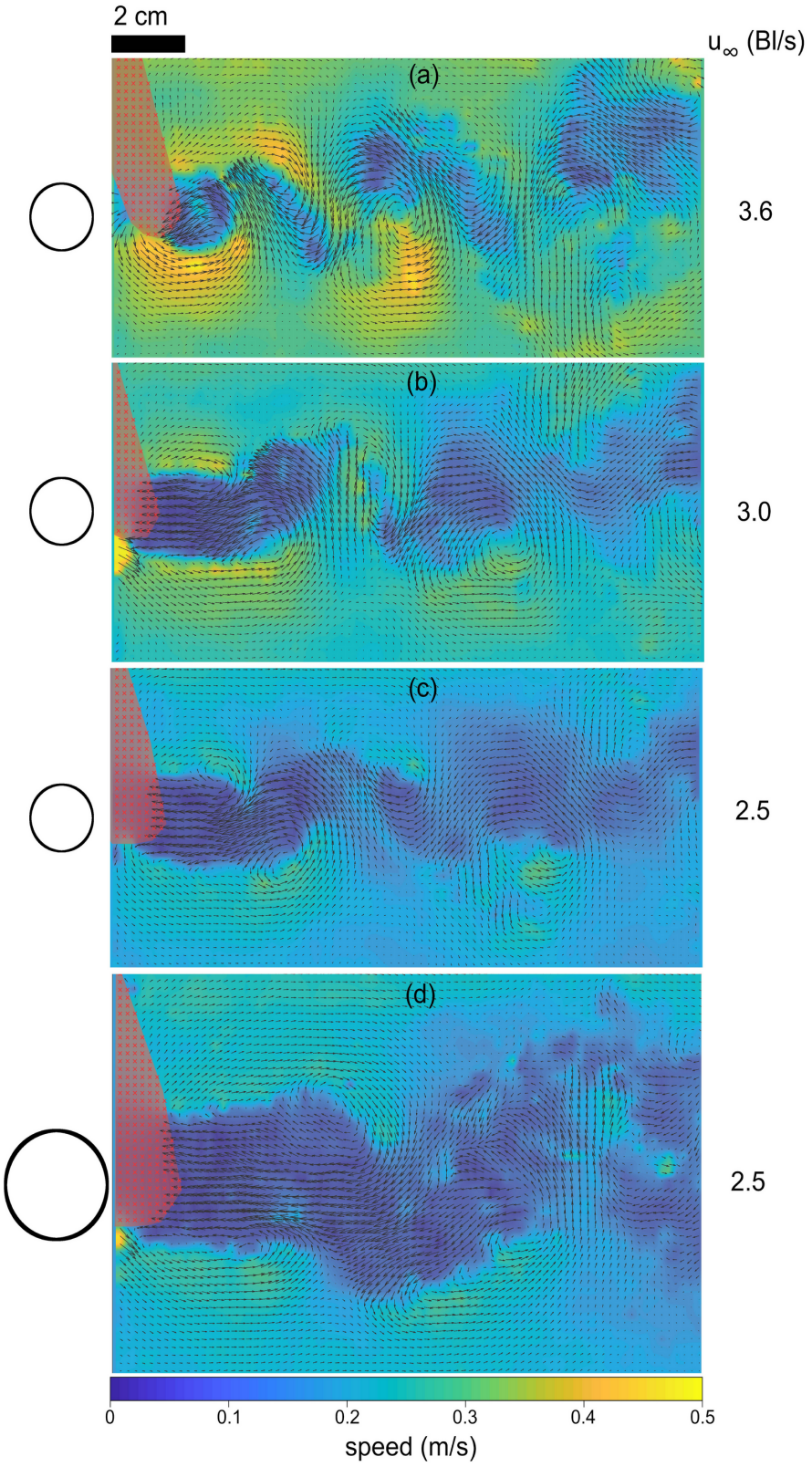

Figure S2. Velocity fields of the wake produced by the small cylinder (a-c) and the large fixed cylinder(d).

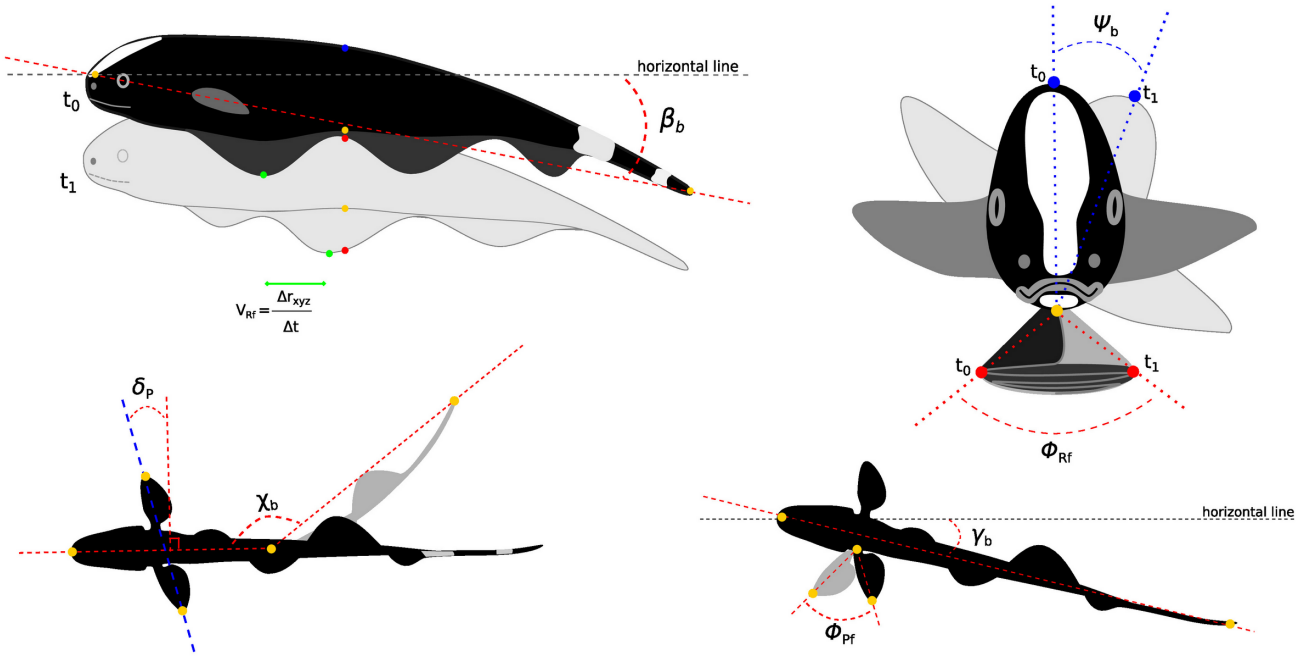

Figure S3. Digitized points used for calculating pitch β_b, roll Ψ_b, yaw γ_b, Ribbon fin wave amplitude Φ_{Rf}, Pectoral fin stroke frequency n_{PF}, Pectoral fin stroke amplitude Φ_{pf}, pectoral fin asymmetry δ_P, *and* body bending χ_b. Ribbon fin wave length λ_{RF} was calculated using the ribbon fin wave speed V_{RF} divided by ribbon fin frequency.

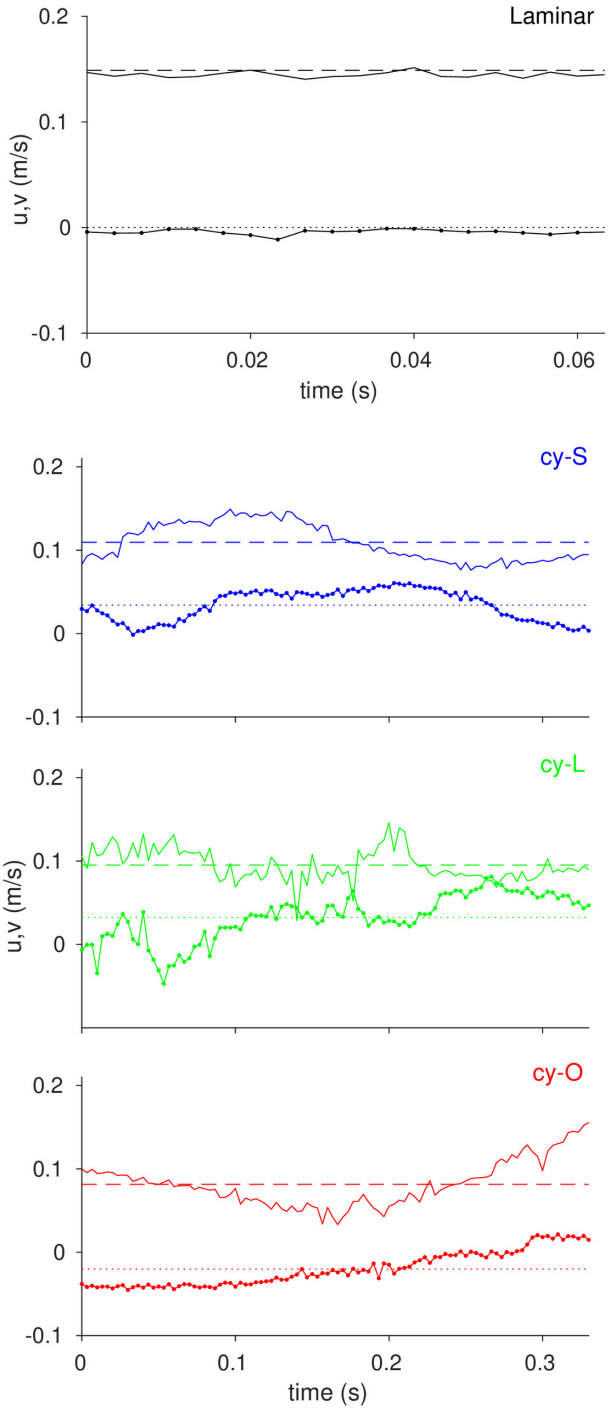

Figure S4. Time series of flow speed components (u and v) downstream for laminar conditions, small cylinder (cy-S), large cylinder (cy-L) and oscillating cylinder (cy-O) at 1.8 Bl/s.

Table S1. Kinematic variables versus flow speed. Comparison between linear and non-linear regression models. Linear regression showing 95% CIs. See Fig. 3.

I) Linear vs. Non linear regression models (see Figure 3)

Ribbon fin wave speed		
model	Adjusted R^2	AIC
linear	0.95	170.4
quadratic	0.95	170.5

Ribbon fin wave acceleration		
model	Adjusted R^2	AIC
linear	0.84	481
quadratic	0.84	480

Ribbon fin wave frequency		
model	Adjusted R^2	AIC
linear	0.9	118.6
quadratic	0.9	120.5

Pitch		
model	Adjusted R^2	AIC
linear	0.6	298
quadratic	0.6	289

II) Linear regression results - 95% CI

Ribbon fin wave speed		
	CI low	CI high
intercept	3.5	5.7
x	4.8	5.5

Ribbon fin wave accelerations		
	CI low	CI high
intercept	-90.3	-40.6
x	54.7	70.5

Ribbon fin frequency		
	CI low	CI high
intercept	0.9	2.2
x	1.6	2.1

pitch		
	CI low	CI high
intercept	10.4	18.3
x	-6.6	-4.1

Movie 1. [(00:05 s) Knifefish swimming in laminar conditions. (00:16 s) Fish swimming behind a large and small fixed cylinders. (00:36 s) Fish swimming in laminar, behind the small fixed cylinder and behind the oscillating cylinder. (01:15s) Fish showing passive movements in the wake of an oscillating cylinder. (01:31 s) 3D printed fish model in both the wake of a fixed cylinder and the wake of an oscillating cylinder. (01:49 s) Instantaneous vorticity fields of the ribbon fin of a knifefish swimming in laminar conditions, behind the fixed cylinder and behind the oscillating cylinder].